UNSTEADY TRANSITION MEASUREMENTS
ON A PITCHING THREE-DIMENSIONAL WING

S23-08

160483

N93-27450

Peter F. Lorber and Franklin O. Carta

United Technologies Research Center
East Hartford, CT 06108

ABSTRACT

Boundary layer transition measurements have been made during an experimental study of the aerodynamics of a rectangular wing undergoing unsteady pitching motions. The wing was tested at chordwise Mach numbers between 0.2 and 0.6, at sweep angles of 0, 15, and 30°, and for steady state, sinusoidal, and constant pitch rate motions. The model was scaled to represent a full size helicopter rotor blade, with chord Reynolds numbers between 2 and 6×10^6. Sixteen surface hot film gages were located along three spanwise stations: 0.08, 0.27, and 0.70 chords from the wing tip. Qualitative heat transfer information was obtained to identify the unsteady motion of the point of transition to turbulence. In combination with simultaneous measurements of the unsteady surface pressure distributions, the results illustrate the effects of compressibility, sweep, pitch rate, and proximity to the wing tip on the transition and relaminarization locations.

NOMENCLATURE

A	pitch rate, $\dot{\alpha}c/2U_c$
c	airfoil chord (17.3 in.)
C_P	pressure coefficient, $(P - P_\infty)/q$
C_P^*	pressure coefficient for locally sonic chordwise velocity
k	reduced frequency, $\omega c/2U_c$
M_c	chordwise Mach number, $M_\infty \cos \Lambda$
M_∞	freestream Mach number
P_∞	freestream static pressure
q	dynamic pressure, $\frac{1}{2}\rho_\infty U_c^2$
t	time
T	oscillation period
Re	Reynolds number, cU_c/ν
U_c	chordwise component of freestream velocity, $U_\infty \cos \Lambda$
U_∞	freestream velocity
x	distance along chord from leading edge
z	distance along span from tip leading edge
$\dot{\alpha}$	pitch rate, rad/sec
α	geometric angle of attack

ramp: $\alpha = \alpha_{min}, \tau \leq 0.125$

$\alpha = \alpha_{min} + 2(\tau - 0.125)(\alpha_{max} - \alpha_{min}),$
$\quad 0.125 \leq \tau \leq 0.625$

$\alpha = \alpha_{max}, \tau \geq 0.625$

sine: $\alpha = \alpha_0 - \alpha_1 \cos 2\pi\tau$

α_{ss}	steady state stall angle
Λ	sweep-back angle
ν	kinematic viscosity
ρ_∞	freestream density
τ	nondimensional time, t/T
ω	circular frequency, $2\pi/T$

INTRODUCTION

Knowledge of the state of the boundary layer is a prerequisite to understanding the aerodynamics of airfoils and wings in unsteady motion. In particular, the response during dynamic stall (pitching motions penetrating beyond the steady-state stall angle) may differ substantially, depending upon whether the boundary layer prior to separation is laminar or turbulent, completely subsonic or locally supersonic, fully attached or containing regions of reversed flow. The boundary layer state is in turn influenced by the Reynolds and Mach numbers of the external flow, airfoil contours and surface roughness, freestream turbulence level, and the presence of sweep and three-dimensionality.

Numerous investigations of dynamic stall have been conducted, at Reynolds numbers from 10^3 to 10^7, at Mach numbers from essentially incompressible to nearly transonic, and for a wide variety of two- and three-dimensional geometries. Most have concentrated on measurements of either the aerodynamic forces (surface pressures or overall model loads) or the flow field characteristics (using various visualization techniques). Only a few studies have included measurements of the boundary layer state. The most informative approach is to obtain complete boundary layer profiles at numerous stations by means of hot wire anemometry[1] or laser velocimetry.[2] This is usually a difficult and time-consuming process. A simpler approach is to use surface-mounted instrumentation to obtain qualitative characteristics. Sublimation, surface visualization, and shear-sensitive liquid crystal techniques have proven useful in steady or slowly varying flow. For higher frequency ($f \simeq 10$Hz) conditions, and when data can only be efficiently acquired electronically, the surface hot film gage is preferred.[3-5]

This paper presents the results of such surface hot film gage measurements of the state of the boundary layer on a three-dimensional wing model. The model was scaled to be representative of a full scale helicopter main rotor, with Reynolds numbers of $2-6 \times 10^6$. It was tested at freestream Mach numbers between 0.2 and 0.6, and in both swept and unswept configurations. Previous publications[5-10] have described the surface pressure and integrated aerodynamic

load results from the current experiment and from an earlier experiment using a two-dimensional (tunnel-spanning) version of this model. The boundary layer state measurements described in the current paper should contribute to the understanding of the previous results. The measured transition locations should also be useful for computational simulation of the experiment.

DESCRIPTION OF EXPERIMENT

The model was a straight, rectangular, untwisted, semi-span wing of 17.3 in. (44 cm) chord and 48 in. (122 cm) span (Fig. 1). The aspect ratio of a full wing would be 5.6. The wing consisted of a steel spar and fiberglass airfoil panels, and had a Sikorsky SSC-A09 9% thickness cambered section (Fig. 2). Airfoil coordinates have been provided in Ref. 6. The surface was kept smooth, with no artificial roughness added to alter the transition characteristics. The wing was mounted at sweep angles of 0, 15, and 30° from the side wall of the 8 ft (2.4 m) octagonal test section of the UTRC Large Subsonic Wind Tunnel. Additional airfoil panels were added to the spar at non-zero sweep angles in order to keep the wing tip $\frac{1}{4}$ chord at the tunnel centerline. The experiment was conducted at five chordwise Mach numbers, $M_c = 0.2, 0.3, 0.4, 0.5,$ and 0.6. Based upon the model chord and the fact that this wind tunnel is vented to atmosphere in the stilling section, the chord Reynolds numbers for these experiments were approximately equal to $10^7 \times M_c$. Longitudinal turbulence levels have been measured in this facility using an LDV system to be between 0.7 and 1.2% of the freestream velocity[11]. Measurements with an unsteady pitot-static probe during the current experiment indicated root-mean-square unsteadiness equivalent to 0.35–0.5% of the freestream velocity for $0.3 \leq M_c \leq 0.6$, and 0.9% at $M_c = 0.2$.

A hydraulic rotary drive oscillated the model in pitch about the line connecting the root and tip $\frac{1}{4}$ chord. Two
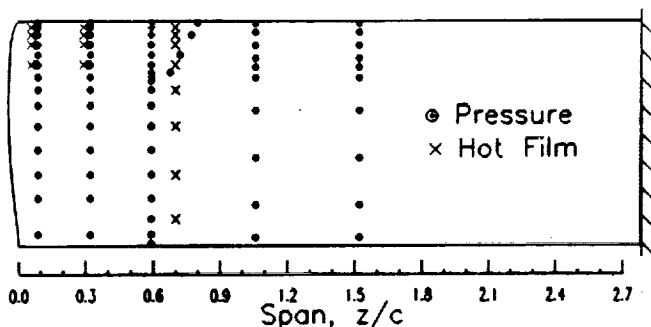

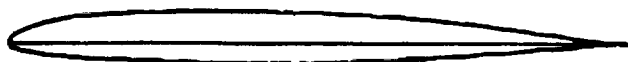Fig. 1. Wing planform and instrumentation locations.

Fig. 2. SSC-A09 airfoil section.

pitching waveforms were used, sinusoids and ramps. The sinusoids were performed at frequencies from 1.25 to 12 Hz ($0.025 \leq k \leq 0.15$), at amplitudes primarily of 6 and 10°, and at numerous mean angles. The ramps began at a steady-state condition (usually $\alpha = 0$), increased at constant rate to a maximum angle, maintained that maximum for a short time, and then returned to the initial condition. The maximum pitch angles were 30° at $M_c = 0.2$ and 0.3, 25° at $M_c = 0.4$, 18° at $M_c = 0.5$, and 13.5° at $M_c = 0.6$. The nondimensional pitch rates were selected between $A = \dot{\alpha}c/2U_\infty$ of 0.001 and 0.025, bounded by a limiting dimensional rate of 560°/sec. Data were obtained for a total of 259 large amplitude sinusoids, 120 ramps, 260 small amplitude sinusoids, and 295 steady-state conditions. The complete data set will be made available in a technical report and a set of digital data tapes.

Unsteady surface pressure measurements were made on the wing model by 112 miniature transducers distributed among five spanwise stations. The suction surface transducer locations are shown by the dots in Fig. 1. The chordwise arrays on the upper surface had 10, 14, or 18 transducers each. The lower surface arrays were less dense, containing 6 or 18 transducers each. The transducers were installed so as to retain a smooth surface contour and achieve a flat frequency response to at least 4 kHz. The pressures were integrated along the chord at each spanwise station to determine the unsteady lift, pressure drag, and pitching moment coefficients.

Sixteen flush-mounted surface hot film gages were used to determine transition and separation locations. As shown by the x-marks in Fig. 1, the gages were located in chordwise arrays at three spanwise stations, $z/c = 0.08, 0.27,$ and 0.70. (Note that $z = 0$ is at the wing tip.) The chordwise stations were $x/c = 0.026, 0.060, 0.103, 0.192, 0.302, 0.464, 0.682,$ and 0.880. All eight chordwise stations were used at $z/c = 0.70$, while only the forward four stations were used at $z/c = 0.08$ and 0.27. The $x/c = 0.026$ and 0.103 gages at $z/c = 0.70$ were offset by 1 in. (to $z/c = 0.65$) to reduce the chance for thermal interference. TSI model 1268 gages were installed in holes drilled through the fiberglass airfoil skins. Each gage consists of a heated element deposited on the end of a 0.15 in. (0.38 cm) diameter quartz rod. The hot films were operated in the constant-temperature mode, at a nominal operating temperature of 225 C, corresponding to an overheat ratio (hot to cold gage resistance) of 1.35. The output voltage will increase with the heat transfer from the gage, and therefore, by the Reynolds analogy, with the shear stress at the wall. The anemometer circuits were mounted immediately outside of the wind tunnel wall to minimize lead resistance and noise.

The output voltages from both the pressure transducers and hot film gages were passed through a 10 kHz low pass filter, and digitized (to 15 bit accuracy) at a rate of 1024 samples per oscillation period (T). Ensemble-averaged time histories were computed using data from 20 pitching oscillations. Both the individual oscillations and the ensemble averages were recorded on digital magnetic tape.

The hot film results were intended to provide only qualitative information on transition and separation locations. When the flow over the hot film gage is laminar, the heat transfer is generally low, with little random unsteadiness. Movement of transition past the gage is indicated by a rapid rise in heat transfer, accompanied by an increase in the higher frequency, random portion of the signal. Separation is indicated by a low level of average heat transfer, but a high level of unsteadiness. Interpretation of hot film signals is simplified in a periodic unsteady flow because the changes from one flow state to another can be more readily identified than the characteristics of a steady-state flow. It is particularly difficult to determine if an individual signal with moderate unsteadiness is turbulent, separated, or transitional.

No attempt was made to obtain quantitative values of skin friction. Calibration of multiple surface mounted gages for unsteady flow is quite difficult, because of the need to either a) calibrate all probes in a reference unsteady flow prior to installation, b) provide a reference flow at each probe, or c) calibrate the probes by comparison to a traceable and portable reference probe. Surface-mounted quartz substrate gages (such as used here) have been shown to have limitations in unsteady flow, including different steady and unsteady calibrations[12,13] The difficulties are created because heat is transferred not only from the active element to the fluid, but also from the element to the substrate, from the substrate to the model, and from the substrate to the fluid. The characteristic lengths and times for these various processes differ, resulting in different steady and unsteady responses.[12] Surface gages with a cavity below the heated element have been more successful in obtaining quantitative unsteady data.[14,15] The qualitative information at the relatively low frequencies (1-10Hz) of interest here should, however, be valid.

Transition information may also be obtained from the surface pressure data. As described in Refs. 1, 5, 6, and 16, transition is frequently accompanied by an increase in the higher frequency random component of the pressure, and by a small shift in the ensemble-average. The problem with this technique is that transition is not the only source of such pressure changes. The pressure information is most useful in confirming or extending transition information obtained from other means. For example, several hot film gages were not operating properly during the unswept portion of this experiment. The data from adjacent pressure transducers was used to cover the resulting gaps between functional hot films. Comparison between hot film and pressure information at other stations confirmed that the pressure changes were actually caused by transition.

STEADY CHARACTERISTICS

For each steady (fixed α) condition, hot film gage voltages were recorded over a 5 second period and averaged. Results for each value of α during a particular test series (at fixed M_c and Λ), were used to form a 'quasi-steady' data
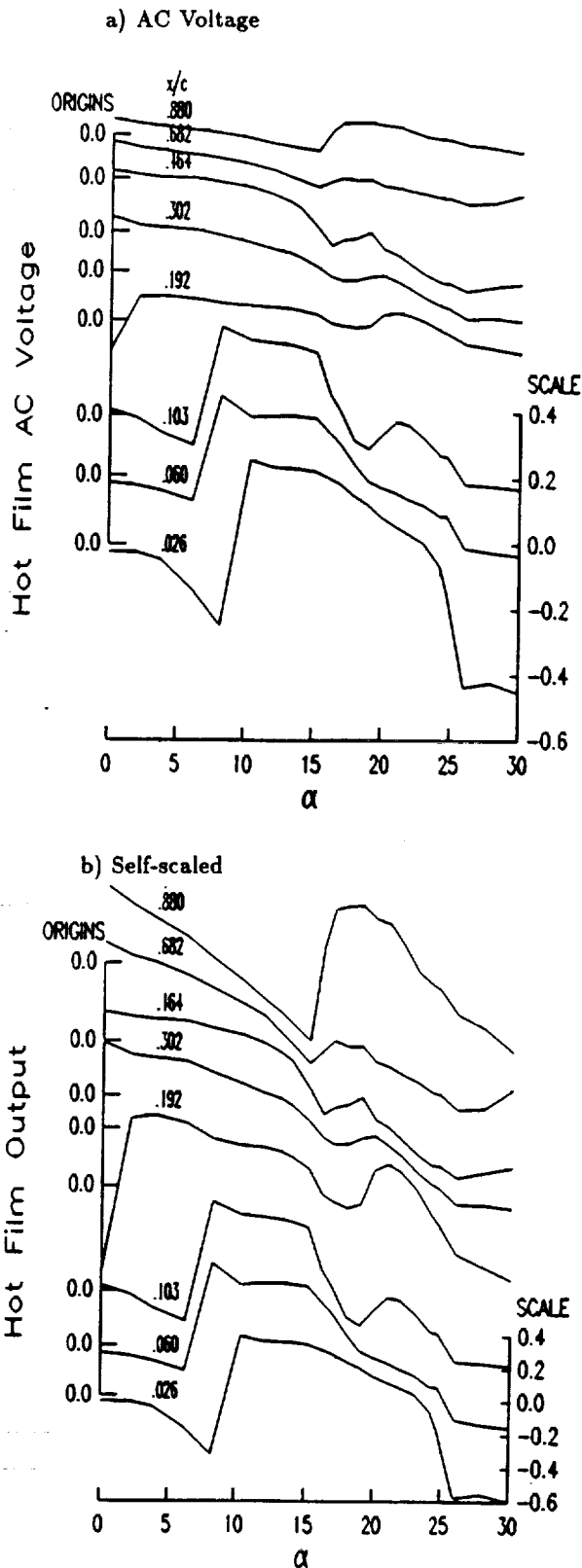

a) AC Voltage

b) Self-scaled

Fig. 3. Steady hot film results at $M_c = 0.3$, $\Lambda = 30$, and $z/c = 0.7$.

file containing hot film outputs as a function of α. Figure 3 shows an example for $M_c = 0.3$ and $\Lambda = 30°$. The results for the 8 gages at $z/c = 0.7$ (the station furthest from the wing tip) are shown in two formats: as AC voltages (Fig. 3a)

and self-scaled to a peak-to-peak value of 1 (Fig. 3b). The AC voltage illustrates the magnitude of the output variations, while the self-scaled output allows regions of change to be easily identified and provides a clear qualitative picture. (Since the gages are not calibrated, quantitative comparisons between gages are not possible.) The origins for the output at each chordwise position (x/c) are along the left of the figure, and the scale is at the lower right. Because data points were only acquired every 1 or 2°, the quasi-steady series appear somewhat rough.

At x/c = 0.026 the sharp increase in heat transfer corresponding to the passage of the transition point over the gage occurs between $\alpha = 8$ and $10°$. Similar sharp increases are also present for the x/c = 0.06, 0.10, and 0.19 gages, but at successively lower values of α. This indicates that at $\alpha = 0$, transition occurs between the x/c = 0.19 and 0.30 gages, and as α increases the transition point moves forward, occurring upstream of the x/c = 0.026 gage for $\alpha \geq 10°$. Away from transition, the heat transfer decreases with increasing α in both laminar and turbulent regions prior to separation. This decrease is a consequence of the thickening of the boundary layer. It is present for $0 \leq \alpha \leq 8°$ and $10° \leq \alpha \leq 20°$ at x/c = 0.026, and at $\alpha \leq 15°$ for x/c = 0.682.

Separation is manifested by the sharp drop in heat transfer that occurs after $\alpha = 15°$, most noticeably at x/c = 0.06, 0.10, and 0.19. This sharp drop does not occur at the x/c = 0.026 station until $\alpha = 25°$. On the aft portion of the wing, where the boundary layer is never laminar, the self-scaling emphasizes a 'bump' of increased heat transfer that occurs while the separation process is underway (between its initiation at $\alpha \simeq 15°$ and completion at $\alpha \simeq 26°$. A possible explanation is that the turbulent boundary layer near the trailing edge is already quite thick at $\alpha = 15°$, and in fact may have thin regions of reversed flow. The resulting heat transfer from the hot film gages would be quite low. The vorticity shed during separation energizes the trailing edge flow, increasing the heat transfer. Once the process is completed and the flow has separated over the entire section, the average output returns to a low level. (The random variations, not shown here, remain high.)

A more quantitative picture of the effect of changes in Mach number, sweep angle, and spanwise position on steady flow transition is provided in Fig. 4. The symbols represent the angle of attack, α, at which the transition point moves past the hot film gage at each chordwise position, x/c. The selected value of α was that corresponding to the most rapid increase of hot film output, which generally occurred 20–40% of the way from the start to the finish of the transition process. Figure 4a illustrates the effect of Mach number at fixed spanwise position (z/c = 0.70) and sweep angle ($\Lambda = 30$). At $M_c = 0.2$ transition occurs near x/c = 0.3 at $\alpha \simeq 0$, and moves forward of x/c = 0.026 by $\alpha = 10°$. At $M_c = 0.3$ transition is always forward of x/c = 0.3, and moves past the x/c = 0.19, 0.10, 0.06, and 0.026 gages at somewhat lower angles of attack than at $M_c = 0.2$. This trend continues at $M_c = 0.4$, as transition always occurs before x/c = 0.19,
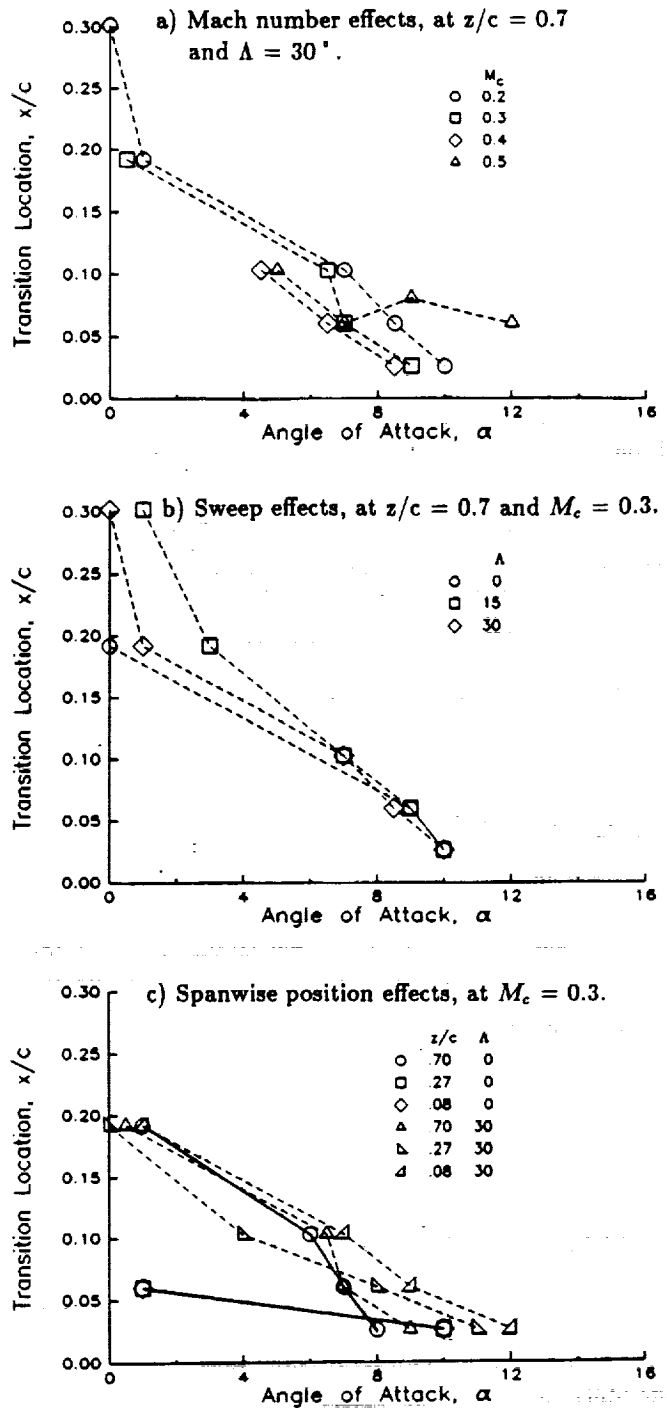

a) Mach number effects, at z/c = 0.7 and $\Lambda = 30°$.

M_c
○ 0.2
□ 0.3
◇ 0.4
△ 0.5

b) Sweep effects, at z/c = 0.7 and $M_c = 0.3$.

Λ
○ 0
□ 15
◇ 30

c) Spanwise position effects, at $M_c = 0.3$.

	z/c	Λ
○	.70	0
□	.27	0
◇	.08	0
△	.70	30
▲	.27	30
◁	.08	30

Fig. 4. Mach number, sweep angle, and spanwise position effects on transition locations in steady flow.

and moves forward of x/c = 0.026 at $\alpha \simeq 8.5°$, a value approximately 1.5° less than at $M_c = 0.2$. These results are consistent with previous data from the unswept 2-D version of this model at $M_c = 0.2$ and 0.4.[6] The primary difference is that the lower effective angle of attack of the 3-D model (a result of the wing tip vortex[9]) delays the forward motion of transition to slightly higher geometric angles. The final data shown on Fig. 4a are at $M_c = 0.5$. The transition point ceases forward motion near x/c = 0.06 at $\alpha \simeq 7°$. The shock effects responsible for this will be discussed in the section on Mach number effects on unsteady transition.

Figure 4b illustrates the effect of sweep angle for fixed spanwise location ($z/c = 0.7$) and Mach number ($M_c = 0.3$). At lower angles of attack ($\alpha \leq 6\degree$), transition is delayed by non-zero sweep. At $\alpha = 0$ transition on the swept wing occurs near $x/c = 0.3$, approximately 10% of chord further downstream than at $\Lambda = 0$. The forward motion of transition is delayed by up to $3\degree$ in α at $\Lambda = 15\degree$, and by up to $1\degree$ at $\Lambda = 30\degree$, in comparison to the $\Lambda = 0$ results. As α increases this difference is reduced. The motion of the transition point past the $x/c = 0.026$ gage occurs at $\alpha \simeq 10\degree$ for all three sweep angles.

The effect of spanwise position is illustrated in Fig. 4c at fixed Mach number ($M_c = 0.3$) and at two sweep angles ($\Lambda = 0$ and $30\degree$). At $\Lambda = 0$ (the solid lines) there is a substantial difference between the inboard ($z/c = 0.7$) and tip ($z/c = 0.27$ and 0.08) stations. Compared to the inboard results, transition near the tip occurs further forward (at $x/c \simeq 0.06$) at low α but moves forward more slowly (passing $x/c = 0.026$ at $2\degree$ higher α). Several mechanisms appear to be involved. Proximity to the wing tip implies proximity to the tip vortex, which reduces the effective angle of attack. This would tend to delay forward motion of transition. In contrast, transition may be promoted by the three-dimensionality and unsteadiness introduced by the tip vortex. It is possible that at low α this second mechanism causes early transition, while the forward motion of transition is delayed by the reduced effective angle of attack. These differences do not appear at $\Lambda = 30\degree$, or at $\Lambda = 15\degree$ (not shown). This is plausible since the tip vortex has less influence on the aerodynamic loading when the wing is swept.[9]

UNSTEADY TRANSITION

The simplest example of transition in unsteady flow is provided by data obtained during constant pitch rate ramps. Figure 5 shows ensemble averaged hot film and pressure time histories for an $\alpha = 0$ to $30\degree$ ramp at $M_c = 0.2$, $\Lambda = 15$, and $A = 0.005$. The series of pressure coefficient time histories at $z/c = 0.59$ shown at the left of the figure show a smooth increase in pressure until an abrupt separation occurs at a nondimensional time of $r = 0.45$ (corresponding to $\alpha = 20\degree$). After separation a negative pressure peak associated with the dynamic stall vortex travels aft along the chord. This is followed by a region of constant pressure indicating massive separation. Further details on the pressure measurements during dynamic stall are provided in Refs. 6, 9, and 10.

The corresponding hot film time gage time histories at $z/c = 0.7$ are shown at the lower right of Fig. 5. Note that because data are acquired 1024 times over the period, T, the temporal resolution of the unsteady measurements is much greater than that of the quasisteady measurements (Fig. 3). Thus the movement of transition past the gages
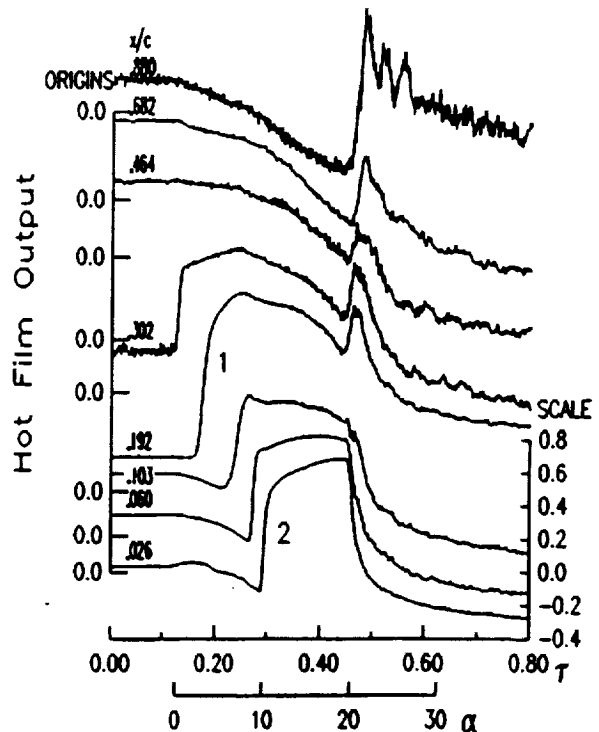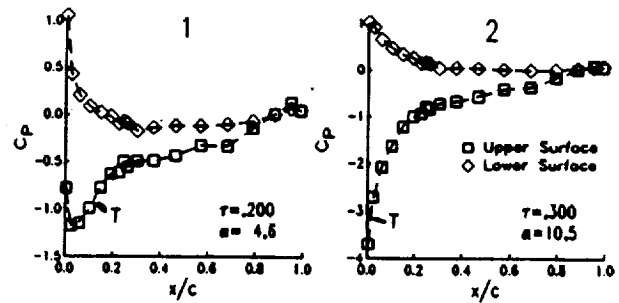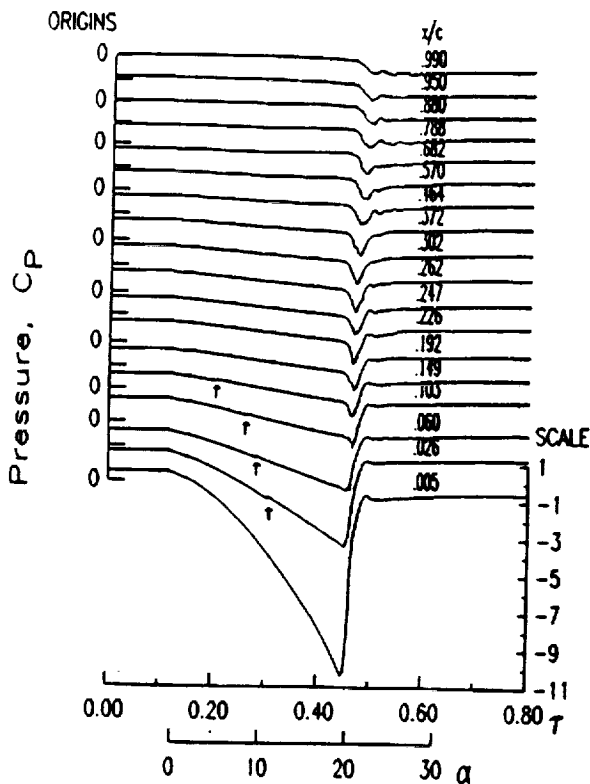

Fig. 5. Pressure and hot film time histories and chordwise pressure distributions at $M_c = 0.2$, for a ramp at $A = 0.005$, $\Lambda = 15\degree$, and $z/c = 0.7$.

is very sharply defined. Over the initial (steady state, $\alpha = 0$) portion of the cycle, transition occurs just aft of the x/c = 0.30 gage, but once the pitching motion begins at $\tau = 0.125$, transition immediately moves forward. The motion continues until $\tau = 0.3$ ($\alpha \simeq 10°$), when transition occurs ahead of the x/c = 0.026 gage. As shown by the chordwise pressure distributions at $\tau = 0.2$ (number 1 in Fig. 5) and at $\tau = 0.3$ (number 2), transition (indicated by the 'T') typically occurs shortly after the suction peak. This is in agreement with the experimental and theoretical work reported in Ref. 17 for incompressible flow over airfoils at a Reynolds number range of $10^5 \leq Re \leq 10^6$. The strong adverse pressure gradient downstream of the suction pressure peak was found to induce transition within 1–2% of chord aft of the peak.

The series of arrows on the pressure time histories (the left portion of Fig. 5) indicate local pressure increases that approximately correspond to the transition measurements obtained with the hot film gages (the right portion of the figure). The pressure increases are quite small, and are only apparent between x/c = 0.026 and 0.149. They generally occur slightly after the hot film gage output rises, i.e. when transition is complete.

The results in Fig. 5 indicate that transition has moved very close to the leading edge by $\tau = 0.3$, well before the onset of separation at $\tau = 0.45$ ($\alpha = 20°$). There is no indication of a significant transitional separation bubble. This implies that dynamic stall for the SSC-A09 section at Reynolds numbers greater than 2×10^6 is a result of turbulent boundary layer separation. This differs from the observations reported in Refs. 1 and 2, for the NACA 0012 airfoil at lower Reynolds numbers (approximately $3–5 \times 10^5$). For those conditions, the transitional separation bubble appears to be a key participant in the dynamic stall process. The sequence observed in the current experiment, laminar boundary layer - turbulent boundary layer - separation, has also been observed during other high Reynolds number experiments, such as Refs. 3 and 4. The separation process for the current model is discussed at greater length in Ref. 10.

The preceding paragraphs have described the general behavior of transition during an unsteady pitching motion. This behavior is similar to that observed at other pitch rates, sweep angles, spanwise positions, and Mach numbers (at least when local supersonic flow effects are minimal). The actual location of the transition point, and its motion as α is increased is, however, dependent on all of these parameters. These dependencies will be discussed next.

Pitch Rate Effects

The effect of pitch rate on the location of transition is illustrated in Fig. 6. Figure 6a shows results at the inboard station, z/c = 0.7, for ramps at a series of five pitch rates between A = 0.001 and 0.02, at fixed Mach number ($M_c = 0.3$) and sweep angle ($\Lambda = 0$). Steady results are also included. Note that the results at x/c = 0.10 and 0.149 were obtained using RMS pressure data, because of the problems with the 0.10 hot film gage described above. (There is no
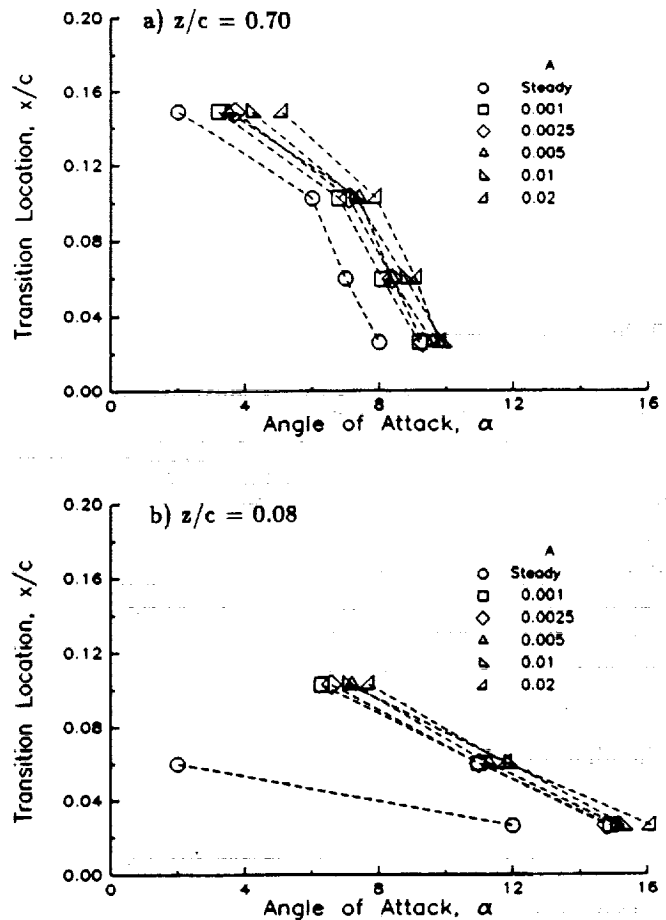

Fig. 6. Effect of pitch rate on transition locations for ramp motions at $M_c = 0.3$, and $\Lambda = 0$.

hot film at x/c = 0.149). The primary effect of increasing the pitch rate is to delay forward motion of the transition point. There is a delay of approximately 0.8° between the steady and A = 0.001 conditions, and an additional delay of approximately 1.2° from A = 0.001 to A = 0.02. The unsteady delays are consistent with the results for the 2-D model[6]. Data at z/c = 0.027 and at other pitch rates and sweep angles (not shown) exhibit similar lags with increased pitch rate.

Close to the wing tip, at z/c = 0.08 (Fig. 6b), there is still a transition delay associated with increased pitch rate, but there is also a a substantial difference between the steady and unsteady response. In steady flow the transition point moves from x/c = 0.06 at $\alpha \simeq 2°$ to x/c = 0.026 at $\alpha = 10°$. This behavior has been discussed above in connection with Fig. 4c. In unsteady flow transition occurs considerably further aft, between x/c = 0.10 and 0.19 at low α, and moves forward of x/c = 0.026 only at $\alpha = 15–16°$, a delay of at least 5° compared to the steady results. Since the relatively early transition in the steady flow was attributed to unsteadiness and three-dimensionality associated with the tip vortex, it is possible that these disturbances do not develop rapidly enough during the unsteady ramp to cause early transition.

Sweep Effects.

Figure 7 illustrates the effect of sweep angle on the transition location during ramps at A = 0.01 and M_c = 0.3. At the inboard location of z/c = 0.70 (Fig. 7a), the effect of sweep appears limited to a somewhat earlier transition at low α for the unswept wing. For $\alpha \geq 8°$, the transition location exhibits no dependence on sweep. This is consistent with the steady-state, M_c = 0.2 data shown in Fig. 4b, and with pressure data[9] showing little effect of sweep on the inboard portion of the wing prior to stall. At z/c = 0.08 (Fig. 7b) sweep effects are more significant. Transition on the unswept wing occurs further forward for $\alpha \leq 8°$, and further aft for $\alpha \geq 10°$. This is also consistent with the steady-state results (Fig. 4c).

Mach Number Effects.

The effect of Mach number will be illustrated using ramp data for the Λ = 15° wing, at a nondimensional pitch rate of A = 0.005, and at the z/c = 0.70 station. Ensemble averaged hot film time histories and instantaneous chordwise pressure distributions will be discussed at M_c = 0.2, 0.3, 0.4, 0.5, and 0.6. This sweep angle and spanwise position was selected for in-depth discussion because the spanwise variations appear relatively low. The pitch rate of 0.005 was selected because it was the highest value that was within
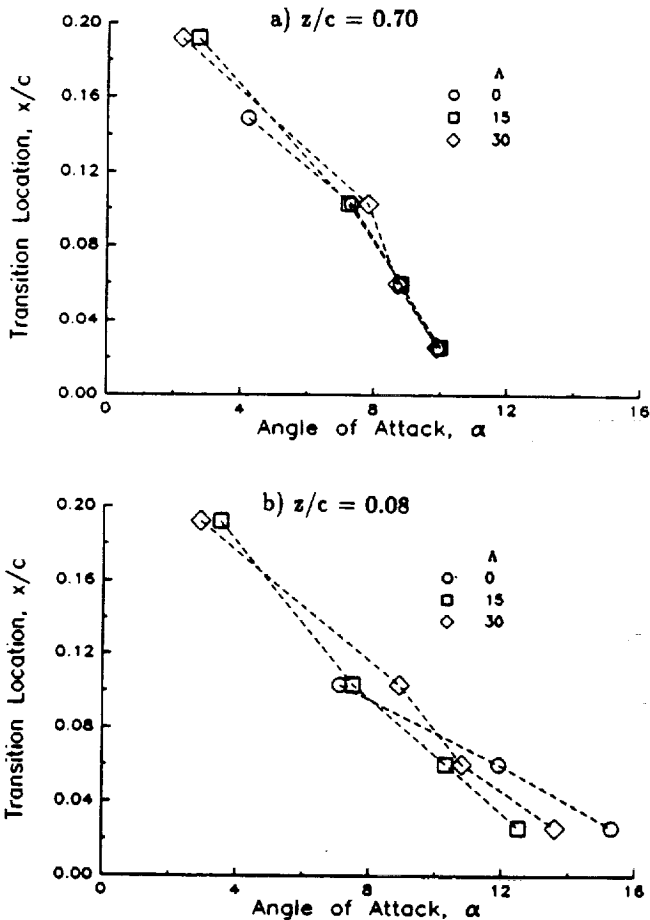
the drive system limits at all Mach numbers. Qualitatively similar variations with M_c were measured at other test conditions.

At M_c = 0.3 (Fig. 8) the results are generally similar to those already described at M_c = 0.2 (Fig. 5), with two differences. The first is that the initial transition location is somewhat further forward, near the x/c = 0.19 gage rather than at the x/c = 0.30 gage. As shown by the chordwise pressure distribution at τ = 0.2 (α = 4.7°, number 1 in Fig. 8), the transition location (indicated by the 'T') is still slightly downstream of the suction peak. A more interesting difference from the M_c = 0.2 results is the rapid drop in hot film output prior to transition present at x/c = 0.026. This drop is sharper than the gradual reduction that typically occurs as increases in α cause the boundary layer to thicken and thereby reduce the heat transfer. More rapid reductions tend to occur at $M_c \geq 0.3$, both in the current experiment and also in the earlier two-dimensional unswept experiment[6]. The cause appears to be compressibility. The minimum hot film output is at τ = 0.275 and α = 9.1°.
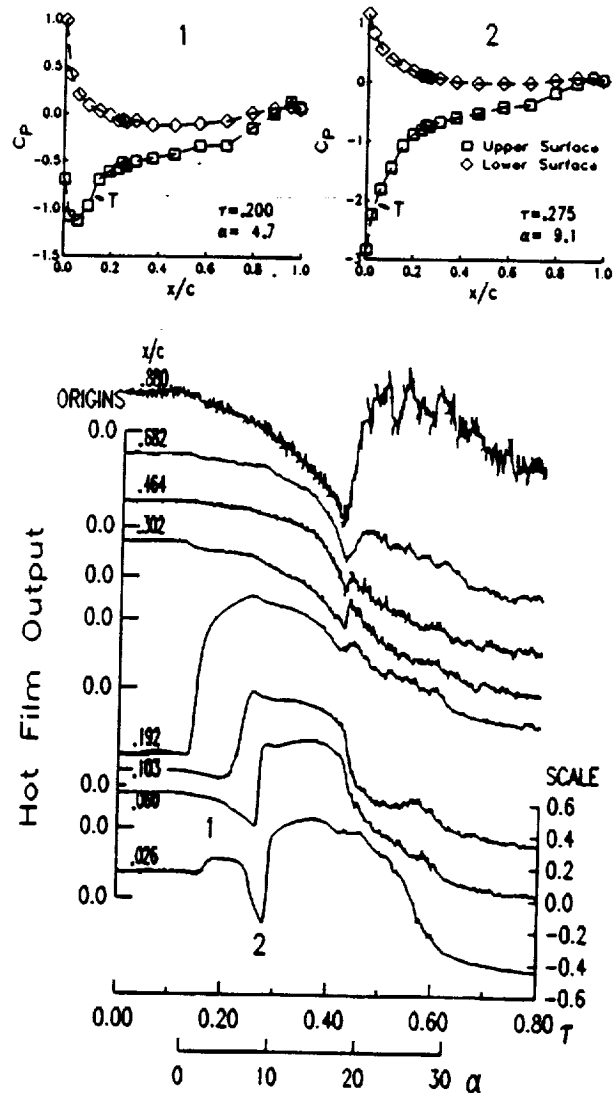

Fig. 7. Effect of sweep on transition locations for ramp motions at M_c = 0.3, and A = 0.01.

Fig. 8. Hot film time histories and chordwise pressure distributions at M_c = 0.3, for a ramp at A = 0.005, Λ = 15°, and z/c = 0.7.

Based upon the measured pressure distribution (number 2 in Fig. 8) and the steady isentropic relations, the maximum local Mach number at this time is approximately 0.6, double the freestream value. Increasing the local Mach number generally increases the temperature, increases boundary layer thickness, reduces the density, and increases the molecular viscosity and thermal conductivity.[18] The first three effects will tend to reduce the heat transfer from the heated element to the air (and therefore to decrease hot film output), while the increase in conductivity will tend to increase heat transfer. The actual balance between the effects in this unsteady, variable pressure gradient flow is not known, but it appears that the effects tending to decrease heat transfer are stronger. There is in general a good correlation between rapid drops in hot film output and regions of high subsonic local Mach numbers. No evidence has been found for the other possible cause of the decreased heat transfer, a laminar separation bubble. Neither the surface pressure distributions, the magnitude of random unsteadiness in the hot film and pressure signals, nor limited surface oil flow visualization indicate separation at these low angles of attack ($\alpha \leq 10^\circ$).

At $M_c = 0.4$ (Fig. 9) the drop in the heat transfer near the leading edge prior to transition is more pronounced. The maximum local Mach number at $\tau = 0.35$, the time of minimum hot film output, is 0.83. The sequence of events is quite compressed for this condition. First, the transition point moves forward of $x/c = 0.026$ at $\tau = .37$ ($\alpha = 9.7^\circ$), as shown by pressure distribution number 1 in Fig. 9). Next, the flow becomes locally supersonic at $\tau \simeq 0.4$ ($\alpha = 10.9^\circ$).

This is indicated in pressure distribution number 2 by the C_P^* arrow. The supersonic bubble expands past $x/c = 0.060$ at $\tau = 0.475$ ($\alpha = 13.9^\circ$, pressure distribution number 3), with a maximum local Mach number of 1.27. This is almost immediately followed by separation, as indicated by the loss of leading edge suction starting at $\tau = 0.5$ ($\alpha = 14.9^\circ$, pressure distribution number 4). The separation appears to initiate near $x/c = 0.02–0.10$ (as indicated by the earliest drop in heat transfer). The rapid sequence of transition, supersonic flow, and separation in a very compact region near the leading edge illustrates the complexity of the flow and demonstrates the need for high spatial and temporal resolution in both experimental or computational experiments.

At $M_c = 0.5$ the region of supersonic flow is more extensive, leading to the more complex hot film response shown in Fig. 10. At lower α the flow remains subsonic, and the behavior is similar to that at lower M_c. The transition point moves forward from its initial position near $x/c = 0.19$, and passes $x/c = 0.10$ at $\tau = 0.3$. Pressure distribution number 1 (at $\alpha = 7.1^\circ$) in Fig. 10 illustrates this portion of the cycle. By $\tau = 0.4$ ($\alpha = 8.8^\circ$, pressure distribution number 2), the flow ahead of $x/c = 0.06$ has become supersonic. Although the maximum local Mach number is quite low (1.05) at $\tau = 0.4$, it increases rapidly, reaching a maximum of 1.4 at $\tau = 0.5$ ($\alpha = 12^\circ$, pressure distribution number 3). The hot film time histories reflect the formation of the shock at $\tau \simeq 0.4$ by the rapid drop in heat transfer at the $x/c = 0.026$ gage and the rapid increase in heat transfer at the $x/c = 0.06$ gage. The decrease at the $x/c = 0.026$ gage is similar to the decreases caused by compressibility that were previ-
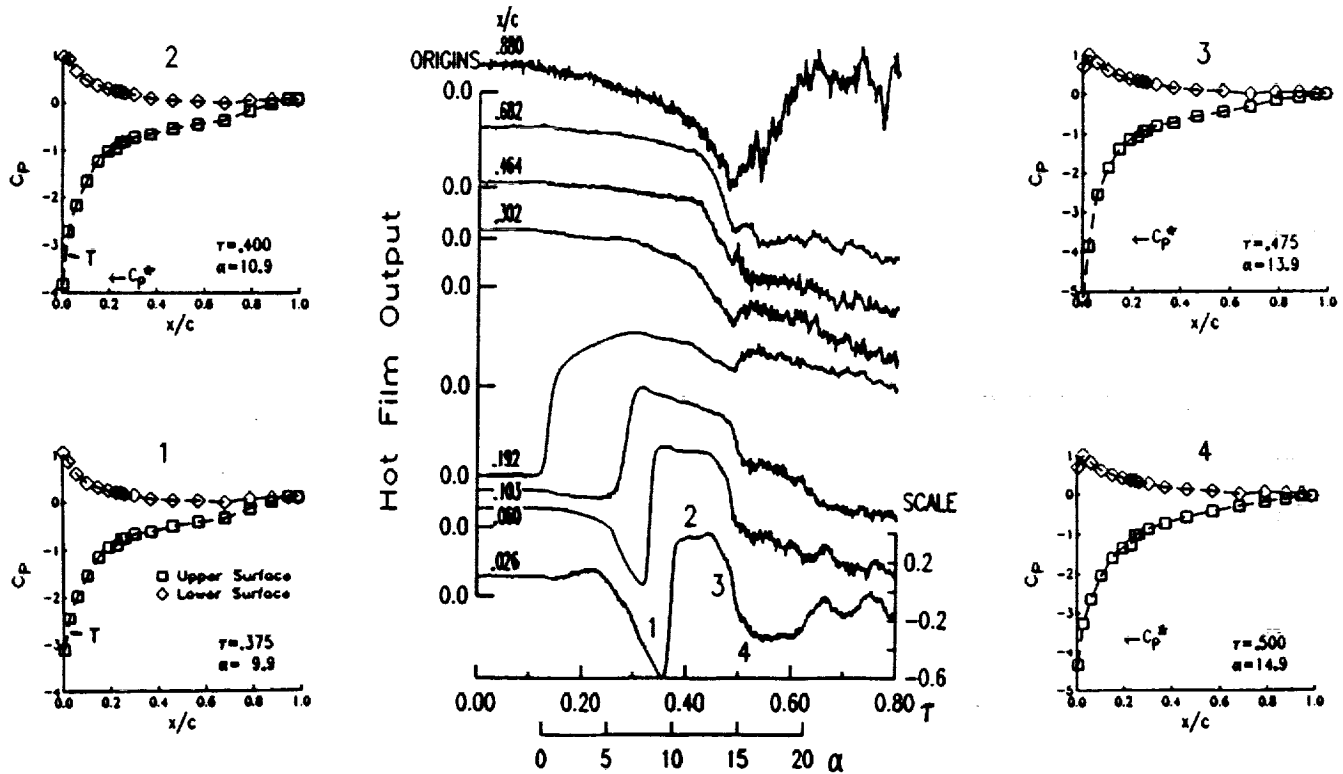

Fig. 9. Hot film time histories and chordwise pressure distributions at $M_c = 0.4$, for a ramp at A = 0.005, $\Lambda = 15^\circ$, and $z/c = 0.7$.
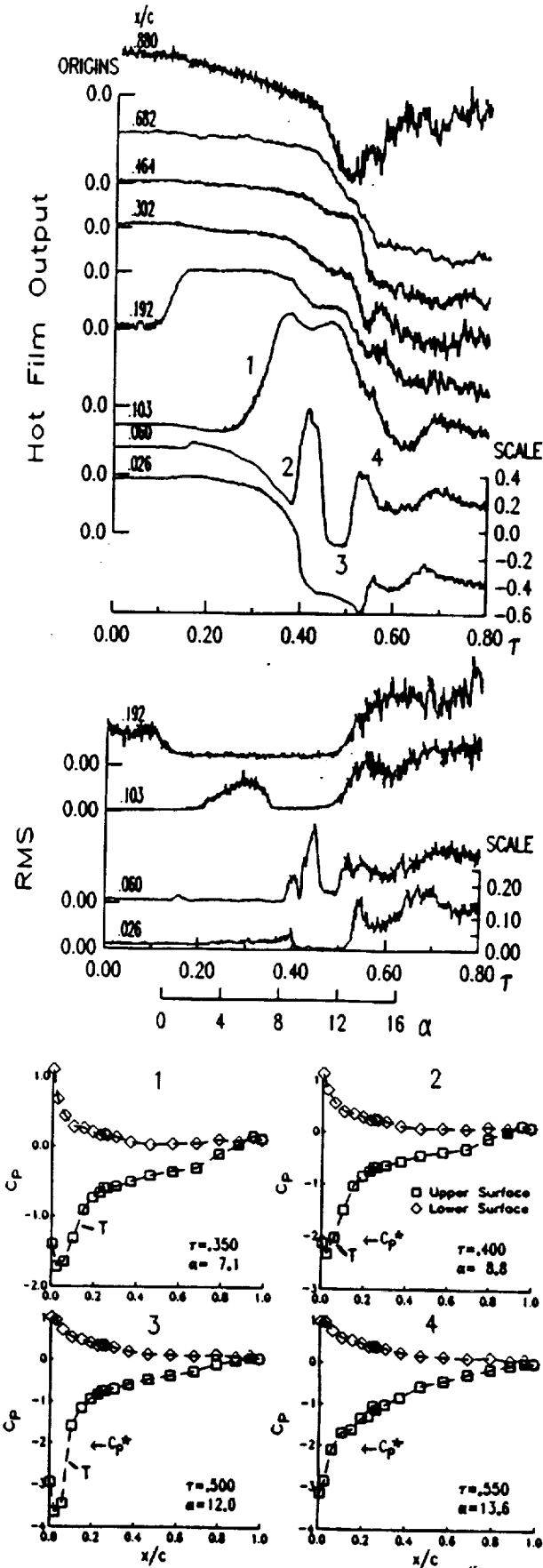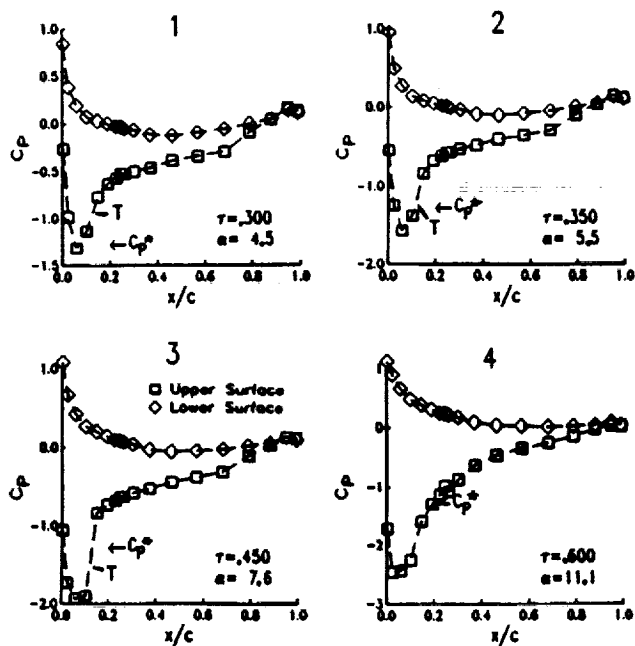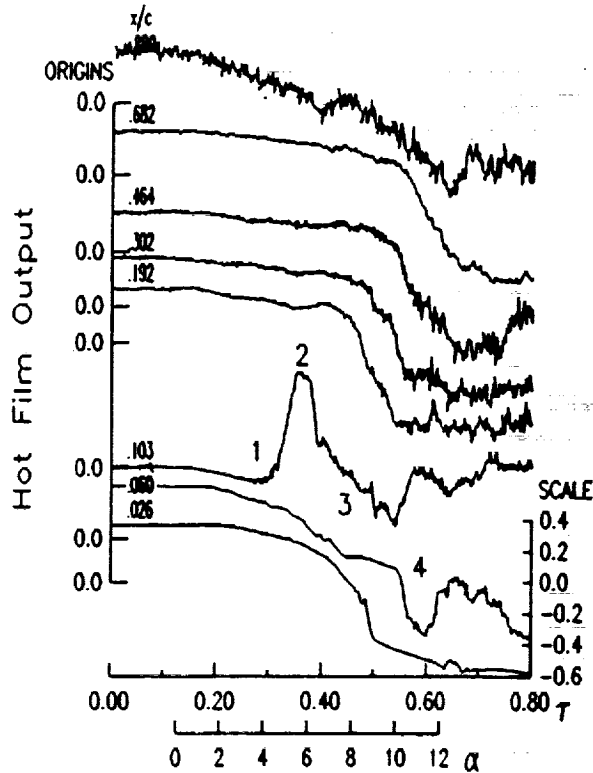
Fig. 10. Hot film time histories and chordwise pressure distributions at $M_c = 0.5$, for a ramp at A = 0.005, Λ = 15°, and z/c = 0.7.

ously described at lower M_c. The increase at x/c = 0.06, which is now downstream of a shock, appears to be a combination of two factors. The first is transition, induced at the shock, and the second is the increase in density behind the shock (a 50% increase is predicted by the normal shock relations). An increase in temperature will also occur behind the shock, tending to reduce heat transfer from the hot film, but the effects of the density increase and of transition are apparently dominant.

As α increases further, the supersonic region expands aft past the x/c = 0.06 gage at $r \simeq 0.45$. The heat transfer from this gage drops since it is now in the supersonic flow ahead of the shock. Pressure distribution number 3 in Fig. 10, at r = 0.5 and α = 12.0°, illustrates this situation. It is likely that the transition point has returned aft with the shock, to between the x/c = 0.06 and 0.10 gages. RMS hot film time histories (shown at the center of Fig. 10) support this hypotheses. The RMS is the variation at each value of r of the data for 20 individual cycles about the ensemble average. The RMS at the x/c = 0.06 gage is considerably lower at $r \simeq 0.4$ and 0.5, when the ensemble averaged output is low (and the flow is presumed to be laminar at this gage), than at $r \simeq 0.425$, when the ensemble averaged output is high (and transition is presumed to be forward of the gage). At r = 0.55 (α = 13.6°, pressure distribution number 4) the boundary layer has begun to separate near the shock. The time and location of the separation are indicated by the initial reductions in heat transfer and suction pressure. Pressure distribution number 4 clearly shows the loss of suction and the disappearance of a sharply defined shock. The flow very quickly becomes massively separated over the entire upper surface. This process is more completely described in Refs. 9 and 10.

At the highest Mach number, M_c = 0.6, compressibility effects are even more dominant. As shown by pressure distribution 1 in Fig. 11, locally supersonic flow begins at $r \simeq 0.3$ and α = 4.5°. Transition occurs between the x/c = 0.10 and 0.19 gages, just aft of the suction pressure peak. Transition moves forward past the x/c = 0.10 gage at r = 0.35 (α = 5.5°, pressure distribution number 2). While the maximum local Mach number at M_c = 0.6 is 1.45, almost the same as the value measured at M_c = 0.5, the supersonic region extends further aft, to x/c = 0.19 at r = 0.45 (α = 7.6°, pressure distribution number 3). As at M_c = 0.5, there is reduced heat transfer from the hot film gage ahead of the shock and increased transfer from the gage behind the shock. Transition is again linked with the shock, and appears to move aft as the supersonic zone strengthens between r = 0.35 and 0.45. Separation occurs starting at $r \simeq$ = 0.55, as indicated by drops in the ensemble averaged hot film output, increased randomness, and the disappearance of a sharply defined shock. This last effect is shown in pressure distribution number 4, at r = 0.6 and α = 11.1°. At M_c = 0.6 the loss of leading edge suction is not as sudden as at M_c = 0.5, and massive separation of the entire upper surface is somewhat delayed. Further details on the separation process are provided in Ref. 10.

The transition results described in this section are summarized in the form of a transition location versus angle of attack plot in Fig. 12. The low angle of attack ($\alpha \leq 4°$) data indicate that as M_c increases, the transition point moves forward earlier. Motion past the x/c = 0.19 gage occurs at approximately 4° earlier at M_c = 0.6 than at M_c = 0.2. The earlier transition at higher M_c may be at least in part a result of increased Reynolds number. At low angle

of attack the adverse pressure gradient aft of the suction peak is relatively weak, so transition may be induced by the amplification of natural disturbances, similar to the process on a flat plate. The concept of a critical Reynolds number based on x, $\frac{U_e x}{\nu}$, is applicable. For the 0.4-1% freestream turbulence levels present in this experiment, a critical Reynolds number of approximately 5×10^5 is likely.[19] The value of x/c yielding this Reynolds number varies from x/c = 0.25 at M_c = 0.2 to x/c = 0.08 at M_c = 0.6. The $M_c \leq 0.4$ data in Fig. 12 are in rough agreement with this trend, but at M_c = 0.5 and 0.6, the experimental transition locations are considerably further aft.

At higher angles of attack ($6 \leq \alpha \leq 10°$), the dependence of the transition location on M_c is reduced (Fig. 12), as long as the regions of supersonic flow are very small and weak. Under these conditions ($M_c \leq 0.4$), transition appears to be initiated by the adverse pressure gradient immediately aft of the suction peak. As shown by the pressure distributions in Figs. 5, 8, and 9, the position of the suction peak does not vary strongly with M_c.

For M_c = 0.5 and 0.6, sizable regions of supersonic flow develop at moderate angles of attack. The shock terminating these regions becomes the initiator of transition. As shown in Fig. 12, at M_c = 0.5 this link between the transition point and the shock causes the forward motion of the transition point to be halted near x/c = 0.06-0.10 at $\alpha \simeq 10°$. At M_c = 0.6, the transition point also remains near the shock (x/c $\geq$ 0.1) for $\alpha \geq 5°$. The chordwise resolution of the hot film measurements is too coarse to determine whether transition occurs immediately following or preceding the shock. The results only indicate laminar conditions forward of the shock and turbulence aft. There is no clear indication of the separation that is the classic response of a laminar boundary layer to the presence of a shock. There is also no evidence of the multiple 'lambda' shocks that are commonly observed with laminar boundary layers.[20,21] It must be emphasized that there are potentially significant differences between the current experiment and the traditional results. This experiment is at a low freestream Mach
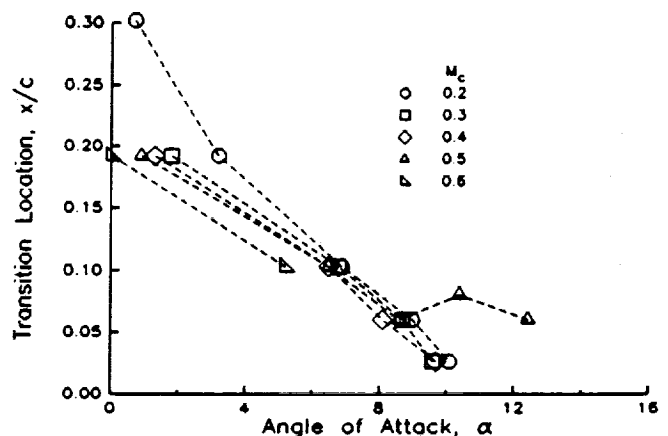
Fig. 11. Hot film time histories and chordwise pressure distributions at M_c = 0.6, for a ramp at A = 0.005, Λ = 15°, and z/c = 0.7.

Fig. 12. Effect of Mach number on transition locations for ramp motions at A = 0.005 and Λ = 15°.

number and moderate angle of attack, generating a thin supersonic region near the highly curved leading edge, while the traditional experiments were typically performed at low angle of attack and higher freestream Mach number, generating a thick region of supersonic flow over the aft (low curvature) region of an airfoil or plate. The combination of a relatively weak shock ($M \simeq 1.3$–1.4), a thin supersonic region, and a curved surface may result in a shock that induces transition, but, at least temporarily, no significant separation. At higher angle of attack ($\alpha \geq 12°$ at $M_c = 0.5$) the dynamic separation process does begin in the vicinity of the shock.[9,10]

TRANSITION AND RELAMINARIZATION DURING SINUSOIDAL MOTIONS

The previous sections have described the transition process at steady state and during constant pitch rate ramps. This section will discuss results obtained for periodic sinusoidal pitching motions. The primary differences are the introduction of a time-varying pitch rate, and a periodic wake. The pitch-down portion of the sinusoidal motion also allows reattachment and relaminarization to be studied.

Figure 13 provides an example of the hot film and pressure results during sinusoidal motion. The conditions are $\alpha = 10° - 10° \cos \omega t$, $M_c = 0.2$, $k = 0.05$, $A = 15°$, and $z/c = 0.7$. The pressure results (Fig. 13a) show a generally smooth response, punctuated by a sharp separation at $\tau \simeq 0.46$. The separation occurs at $\alpha \simeq 19.8°$, after the pitch rate has dropped substantially from its maximum value of $A = 0.009$. The negative pressure peak associated with the dynamic stall vortex propagates aft, followed by a constant pressure region indicating massive separation. Reattachment begins near the leading edge at $\tau \simeq 0.67$ ($\alpha \simeq 15°$).

The hot film time histories (Fig. 13b) are qualitatively quite similar during pitch-up to the ramp results at $M_c = 0.2$ shown in Fig. 5. As with the ramp, the transition point moves forward from $x/c \geq 0.30$ at $\alpha = 0$ past $x/c = .026$ at $\alpha \simeq 10.7°$. The region of low heat transfer caused by separation corresponds to the constant pressure region shown in Fig. 13a. Starting at $\tau \simeq 0.66$, the boundary layer reattaches from the leading edge aft, as shown by the rapid increase in heat transfer at the $x/c = 0.026$, 0.06, and 0.10 gages (Fig. 13b). The high level indicates that the flow reattaches as a turbulent boundary layer. The subsequent drop in heat transfer, starting at the $x/c = 0.026$ gage at $\tau \simeq 0.74$ ($\alpha = 10.9°$), corresponds to a relaminarization of the boundary layer, again moving from the leading edge aft. The relaminarization at $x/c = 0.026$ occurs at approximately the same value of α as transition. This symmetry is not present for separation and reattachment, since at $x/c = 0.026$ separation occurs at $\alpha = 19.8°$ and reattachment at $\alpha = 15°$. The symmetry of transition and relaminarization does not persist through the conclusion of relaminarization. The transition point moves aft past $x/c = 0.30$ at $\tau = 0.97$ ($\alpha = 0.2°$), but does not return forward until $\tau = 0.07$ ($\alpha = 0.9°$).

a) Pressure
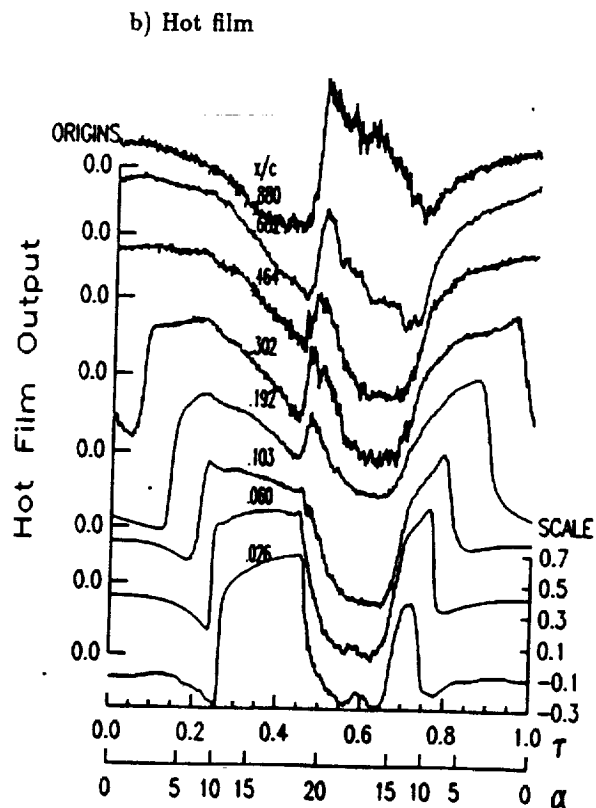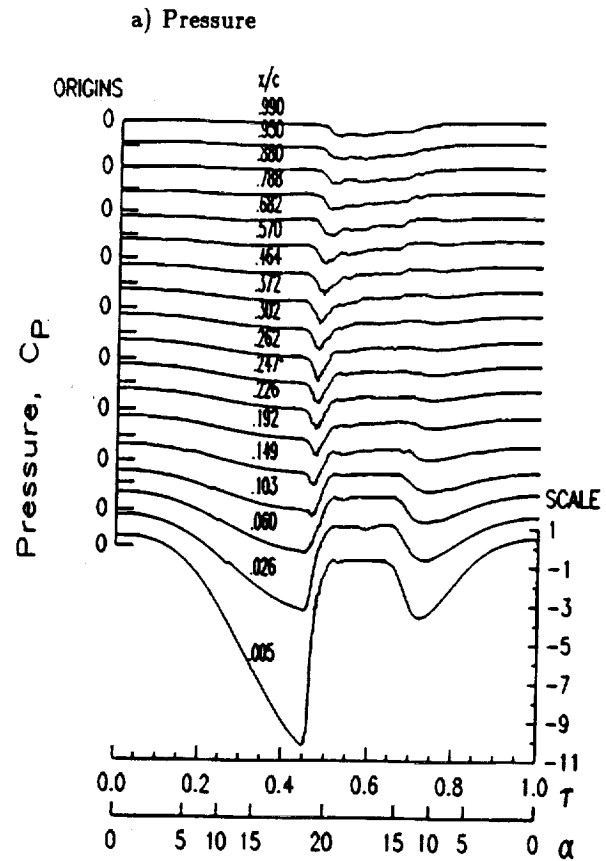

b) Hot film

Fig. 13. Hot film and pressure time histories for sinusoidal oscillation at $\alpha = 10° - 10° \cos \omega t$, $M_c = 0.2$, $k = 0.05$, $A = 15°$, and $z/c = 0.7$.

Transition and relaminarization locations for a series of sinusoidal oscillations at reduced frequencies of k = 0.025, 0.05, 0.1, and 0.15 are shown in Fig. 14. The Mach number, sweep angle, and spanwise position are the same as in Fig. 13. These results show significant hysteresis in the transition-relaminarization cycle at higher frequency. At a given chordwise position, relaminarization generally occurs at a lower α than transition. The largest measured difference is at x/c = 0.19, where data at k = 0.15 show a 3.6° lower relaminarization angle. The hysteresis decreases at higher α, as the transition point approaches the leading edge, to a maximum of 1.8° at x/c = 0.103 and 0.9° at x/c = 0.026. At higher α, transition is primarily influenced by the strong adverse pressure gradient immediately aft of the suction peak. Thus there is less variation in transition location than at lower α, where transition occurs further aft, in a region with a more moderate pressure gradient. The hysteresis observed in Fig. 14 for α = 10° - 10° cosωt motions, in which there are large regions of flow separation, is also present in Fig. 15 for α = 6° - 6° cosωt motions, in which the boundary layers always remain attached. Separation is therefore not an essential requirement for hysteresis.
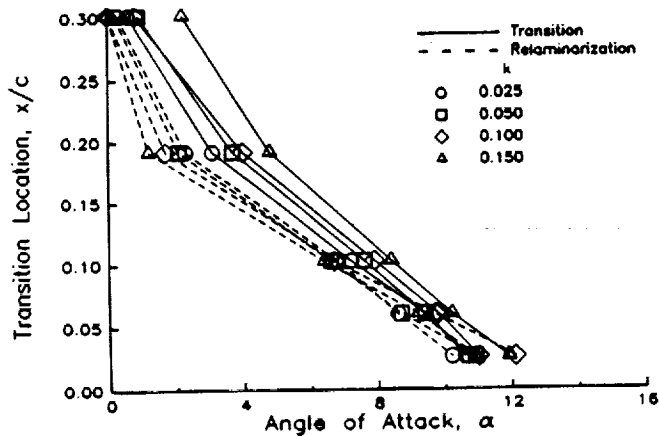
Time histories at higher Mach number, M_c = 0.5, are shown in Fig. 16, for an α = 6° - 6° cosωt oscillation at k = 0.05. The pressure time histories (Fig. 16a) show a flow

a) Pressure

Fig. 14. Transition and relaminarization locations for sinusoidal motions at α = 10° - 10° cosωt, M_c = 0.2, Λ = 15°, and z/c = 0.7.

b) Hot film
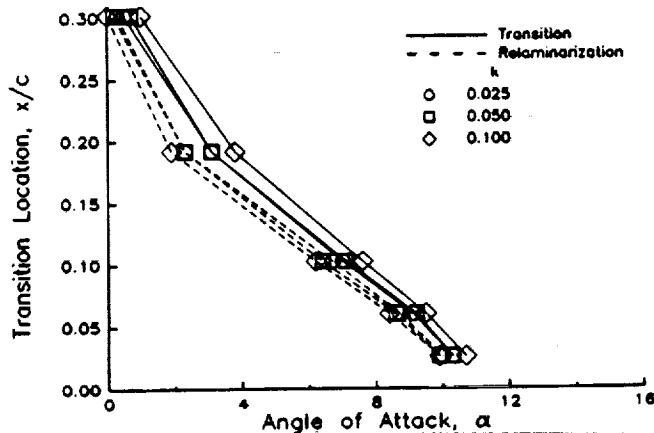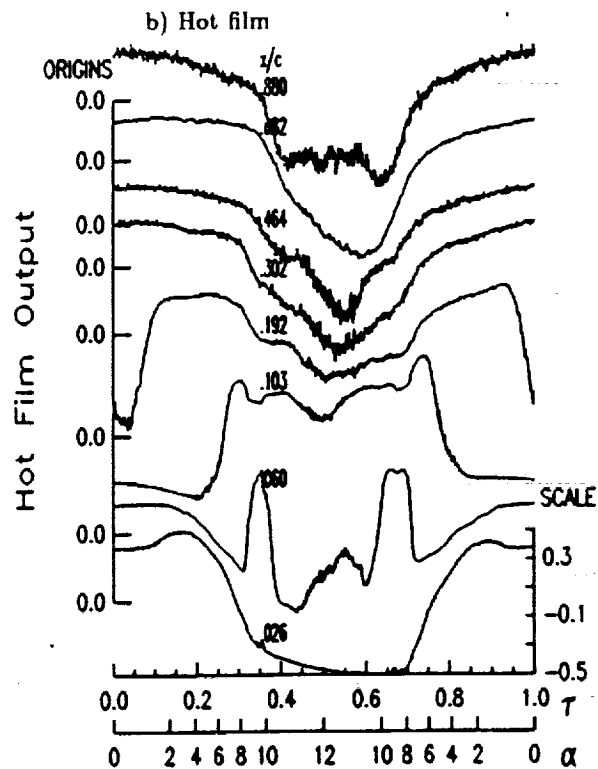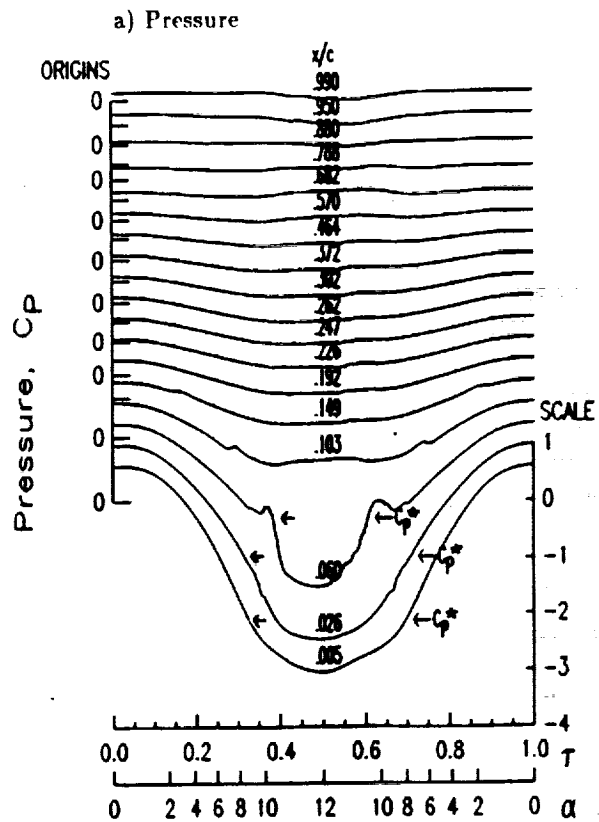

Fig. 15. Transition and relaminarization locations for sinusoidal motions at α = 6° - 6° cosωt, M_c = 0.2, Λ = 15°, and z/c = 0.7.

Fig. 16. Hot film and pressure time histories for sinusoidal oscillation at α = 6° - 6° cosωt, M_c = 0.5, k = 0.05, Λ = 15°, and z/c = 0.7.

that remains attached, but becomes supersonic for x/c = 0.026 and 0.06 at τ = 0.3 and $\alpha \simeq 8$ '. The expansion of the supersonic region and rearward movement of the shock past x/c = 0.06 at τ = 0.38 distorts the pressure time history by creating a rapid pressure drop. The hot film time histories (Fig. 16b) during the pitch-up portion of the cycle appear quite similar to the ramp results at this Mach number (Fig. 10). The increase in heat transfer at the x/c = 0.06 gage between τ = 0.32 and 0.38 correlates closely with the pressure time histories (Fig. 16a), which indicate that the shock forms upstream of x/c = 0.06, and then moves aft past this position. A similar, but reversed, sequence occurs during the pitch-down.

Transition and relaminarization locations are shown in Fig. 17 for M_c = 0.5 sinusoids at k = 0.025, 0.05, and 0.1. As at M_c = 0.2, there is significant hysteresis (up to 1.6 ') involved in the movement of the transition between x/c = 0.19 and 0.06. The differences between the transition and relaminarization angles for $\alpha \geq 9$ ' are reduced to less than 0.5 '. Under these conditions, the shock is believed to be the primary determinant of the transition location.
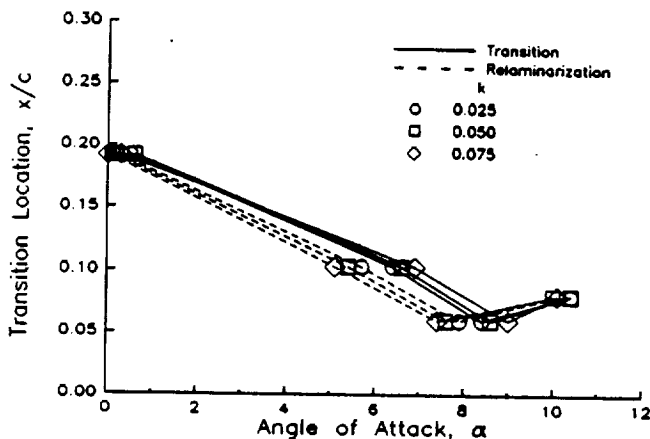

Fig. 17. Transition and relaminarization locations for sinusoidal motions at α = 6 '- 6 ' cosωt, M_c = 0.5, Λ = 15 ', and z/c = 0.7.

CONCLUSIONS

Experimental measurements of transition locations on a rectangular wing model during steady-state and unsteady pitching motions at Mach numbers between 0.2 and 0.6 and Reynolds numbers of 2-6×10⁶ have resulted in the following observations.

1. At low angle of attack ($\alpha \leq 4$ ') transition generally occurs between x/c = 0.14 and 0.3. Transition occurs furthest aft at M_c = 0.2, and closest to the leading edge at M_c = 0.6. Under these conditions, where the adverse pressure gradient is relatively mild, the occurrence of transition may be associated with reaching a critical Reynolds number, based on x, of approximately 5×10⁵.

2. As α is increased, the adverse pressure gradient increases and the transition point moves forward. For $\alpha \geq 6-8$ ', transition occurs a very short distance aft of the suction pressure peak. Under these conditions, the dependence on M_c (and therefore also Reynolds number) is reduced, for $M_c \leq 0.4$. Transition moves forward of the first hot film gage (x/c = 0.026) at $\alpha \simeq 10-12$ '.

3. For the relatively high Reynolds number range of this experiment, the boundary layer becomes essentially turbulent prior to separation. There is no indication of the transitional separation bubble frequently observed at lower Reynolds number.

4. At M_c = 0.5-0.6, significant regions of supersonic flow develop near the leading edge at $\alpha \geq 7-10$ ', with maximum local Mach numbers of 1.3-1.4. Transition is initiated at the shock that terminates the supersonic region at x/c $\simeq$ 0.1-0.15. There does not appear to be any substantial shock-induced separation at these moderate angles of attack.

5. Increasing pitch rate from A = 0.001 to 0.02 introduces a lag in the forward motion of the transition point, by up to $\Delta\alpha$ = 2 '.

6. Wing sweep angles of Λ = 0, 15, and 30 ' do not substantially alter the transition locations at the inboard station (z/c = 0.7 chords from the tip). However, very close to the wing tip, transition occurs earlier for the unswept wing at low α than for the swept wing, possibly because of disturbances induced by the tip vortex.

7. During sinusoidal pitching motions, the transition point moves forward as α increases, and aft as α decreases. At higher reduced frequency, a significant hysteresis of up to 3.6 ' develops between the values of α for transition and relaminarization. The hysteresis is much stronger near x/c = 0.15-0.30 than it is closer to the leading edge.

ACKNOWLEDGMENTS

REFERENCES

1. De Ruyck, J., Hazarika, B., and Hirsch, C., "Transition and Turbulence Structure in the Boundary Layers of an Oscillating Airfoil," Vrije Univ. Brussels Report STR-16, Dec. 1989.

2. Chandrasekhara, M.S., and Ahmed, S., "Laser Velocimetry Measurements of Oscillating Airfoil Dynamic Stall Flow Field," AIAA Paper 91-1799, 22nd Fluid Dynamics, Plasma Dynamics, and Lasers Conference, Honolulu HI, June 1991.

3. Carr, L.W., McCroskey, W.J., McAlister, K.W., Pucci, S.L., and Lambert, O., "An Experimental Study of Dynamic Stall on Advanced Airfoil Sections, Volume 3: Hot-Wire and Hot-Film Measurements," NASA TM 84245, Dec. 1982.

4. Carta, F.O., "Dynamic Stall of Swept and Unswept Oscillating Airfoils, AGARD FDP Symposium on Unsteady Aerodynamics," May 1985.

5. Lorber, P.F., and Carta, F.O., "Airfoil Dynamic Stall at Constant Pitch Rate and High Reynolds Number," *Journal of Aircraft*, Vol. 25, June 1988, pp. 548-556.

6. Lorber, P.F., and Carta, F.O., "Unsteady Stall Penetration Experiments at High Reynolds Number", AFOSR TR-87-1202, April 1987.

7. Patterson, M.T., and Lorber, P.F., "Computational and Experimental Studies of Compressible Dynamic Stall," *Journal of Fluids and Structures*, Vol. 4, 1990, pp. 259-285.

8. Lorber, P.F., and Carta, F.O., "Incipient Torsional Stall Flutter Experiments on a Swept Three-Dimensional Wing," AIAA Paper 91-0935, 32nd Structures, Structural Dynamics, and Materials Conference, Baltimore MD, April 1991.

9. Lorber, P.F., Carta, F.O., and Covino, A.F. Jr., "Dynamic Stall Experiments on a Swept Three-Dimensional Wing In Compressible Flow," AIAA Paper 91-1795, 22nd Fluid Dynamics, Plasma Dynamics, and Lasers Conference, Honolulu HI, June 1991.

10. Lorber, P.F., "Sweep and Compressibility effects on the Dynamic Stall of a Three-Dimensional Wing," AIAA Paper 92-0191, 30th Aerospace Sciences Meeting, Reno NV, Jan. 1992.

11. Willams, M.C., Pratt & Whitney Aircraft Internal Correspondence, September 1988.

12. Haritonidis, J.H., "The Measurement of Wall Shear Stress," *Advances in Fluid Mechanics Measurements*, Lecture Notes in Engineering (ed. M. Gad-el-Hak), Springer-Verlag, pp. 229-261, 1989.

13. Cook, W., "Response of Hot Element Wall Shear Stress Gages in Unsteady Turbulent Flows," AIAA Paper 91-0167, 29th Aerospace Sciences Meeting, Reno NV, Jan. 1991.

14. Houdeville, R., Juillen, J.C., and Cousteix,J., "Skin Friction Measurements with Hot-Element Gages," *Recherche Aerospatiale*, Vol. 1, 1984, pp. 67-79.

15. Flutie, K.J., and Covert, E.E., "Unsteady Measurement of Skin Friction in Adverse Pressure Gradients; A New Approach to a Well-Known Gauge," AIAA Paper 91-0168, 29th Aerospace Sciences Meeting, Reno NV, Jan. 1991.

16. Greff, E., "In-Flight Measurement of Static Pressures and Boundary-Layer State with Integrated Sensors," *Journal of Aircraft*, Vol. 28, pp. 289-299, May 1991.

17. Schlichting, H., *Boundary Layer Theory*, Seventh Edition, McGraw Hill Book Co., New York NY, 1979, pp. 496-502.

18. Ibid., pp. 719-723.

19. Ibid., pg. 476.

20. Ibid., pp. 358-372.

21. Van Dyke, M., *An Album of Fluid Motion*, Parabolic Press, Stanford CA, 1982, pp. 150-152.